A Galerkin-characteristic finite element method for three-dimensional convection-dominated problems

Bassou Khouya[1,*] Mofdi El-Amrani[2,†] Mohammed Seaid[1,3,‡]

[1] *International Water Research Institute, University Mohammed VI Polytechnic, Benguerir, Morocco. FST Tanger, Abdelmalek Essaadi University, Tangier, Morocco*
[2] *Dpto. Matemáticas Applicada, Universidad Rey Juan Carlos, 28933 Móstoles-Madrid, Spain*
[3] *Department of Engineering, University of Durham, South Road, Durham DH1 3LE, UK*

Abstract

We present an efficient Galerkin-characteristic finite element method for the numerical solution of convection-diffusion problems in three space dimensions. The modified method of characteristics is used to discretize the convective term in a finite element framework. Different types of finite elements are implemented on three-dimensional unstructured meshes. To allocate the departure points we consider an efficient search-locate algorithm for three-dimensional domains. The crucial step of interpolation in the convection step is carried out using the basis functions of the tetrahedron element where the departure point is located. The resulting semi-discretized system is then solved using an implicit time-stepping scheme. The combined method is unconditionally stable such as no Courant-Friedrichs-Lewy condition is required for the selection of time steps in the simulations. The performance of the proposed Galerkin-characteristic finite element method is verified for the transport of a Gaussian sphere in a three-dimensional rotational flow. We also apply the method for simulation of a transport problem in a three-dimensional pipeline flow. In these test problems, the method demonstrates its ability to accurately capture the three-dimensional transport features.

Keywords. Three-dimensional convection-diffusion equations; Galerkin-characteristic method; Finite elements; Unstructured grids; Convection-dominated problems.

1 Introduction

In many practical transport problems from engineering and mathematical sciences, the governing equations involve convection-dominated flow systems. This class of problems has important applications in a variety of physical and engineering areas such as weather prediction, ocean circulation, petroleum reservoir among others. The physical phenomena in these areas can be modeled by transport-diffusion equations with the property that the convective terms are distinctly more important than the diffusive terms; particularly when certain nondimensional parameters reach high values. Examples of these parameters include the Peclet number for convection-diffusion equations and the Reynolds number for incompressible Navier-Stokes equations. Furthermore, it is well known that for large values of these parameters, the convective terms are a source of computational difficulties and nonphysical oscillations. In

[*] khouya.bassou@um6p.ma
[†] mofdi.elamrani@urjc.es
[‡] m.seaid@durham.ac.uk

addition, steep fronts and boundary layers are among the difficulties that most of Eulerian finite element methods fail to resolve accurately, see for example [12]. In general, the Eulerian methods use fixed grids and incorporate some upstream weighting in their formulations to stabilize the spatial discretization. As examples of Eulerian methods we mention the Petrov-Galerkin methods, the streamline diffusion methods, discontinuous Galerkin methods and also many other methods such as the high resolution methods from computational fluid dynamics, in particular, the Godunov methods and the essentially non-oscillatory methods, see [3, 19] among others. The main limitation of these methods is the stability conditions which impose a severe restriction on the size of time steps taken in the simulations. Needless to mention that the complexity and the huge memory requirements of such methods make the state of art in this area more advanced for two-dimensional problems than their three-dimensional counterparts.

The modified method of characteristics is second-order accurate in space and time provided the characteristic curves are exactly calculated, compare for example [14, 22]. However, for general convection problems, the accuracy of the method depends on the order of the interpolation procedure used to calculate the departure points and on the time integration procedure. Theoretical analysis of convergence and stability of the Galerkin-characteristic finite element method have been carried out in many studies, see for example [5, 14, 22, 6]. It should be stressed that research works presented in these references have focused on the analysis of the Galerkin-characteristic finite element method with no algorithmic formulation of the method for engineering applications. Furthermore, our present study differs from the investigations reported in [5, 14, 22, 6] in the fact that it focuses on the computational implementation of the method for three-dimensional convection-diffusion equations on unstructured meshes and it also presents a comprehensive numerical assessment of the method using several test problems. The main objective of our work is the development of a highly efficient Galerkin-characteristic finite element method to numerically solve the convection-dominated problems in three space dimensions. The central idea in these methods is to rewrite the governing equations in terms of Lagrangian coordinates as defined by the characteristics associated with the problem under consideration. The time derivative and the advection terms are combined as a directional derivative along the characteristics, leading to a characteristic time-stepping procedure. The Lagrangian treatment in these methods greatly reduces the time truncation errors in the Eulerian methods, see for example [17, 24]. Furthermore, the Galerkin-characteristic finite element method offers the possibility of using time steps that exceed those permitted by the Courant-Friedrichs-Lewy (CFL) stability condition in Eulerian-based methods for convection-dominated problems. A class of Galerkin-characteristic methods for solving two-dimensional problems has been investigated in [5, 14, 22, 9, 8, 7] among others. Solving three-dimensional advection-diffusion problems has also been reported in [4, 11, 13, 25, 10] among others. Most of these references considered linear advection-diffusion problem with constant coefficients or used structured meshes for the spatial discretization. It should be noted that tetrahedral finite elements are attractive because of their flexibility for representing irregular boundaries and for local mesh refinements. It should also be noted that numerical comparisons between the Galerkin-characteristic finite element method and a class of Eulerian finite element methods have been performed in [7] for two-dimensional convection-dominated flow problems and it has been found that the Galerkin-characteristic finite element method is far more efficient than its Eulerian counterparts.

Our objective in this work is to develop an efficient finite element method for solving three-dimensional convection-diffusion equations using unstructured grids. It has been shown that the method is unconditionally stable provided the characteristics are transported by a divergence-free field that is deduced from the flow velocity. The case where the characteristics are transported by a discrete velocity field which is not divergence-free has been studied in [22]. Analysis of a Galerkin-characteristic method using the standard finite difference discretization has been presented in [5] for convection-diffusion equations. In all these references the convergence and stability of the method are proven under the assumption that all the inner products are calculated exactly. Furthermore, the evaluation of the solutions at the departure points in [5, 14, 22] is performed using an L^2 projection on the finite element space. The present study represents a step towards the implementation of an unconditionally stable Galerkin-characteristic method for the solution of convection-dominated problems in three space dimensions. The unconditional stability

of the proposed method is inherited from the use of the method of characteristics for the convection part and a fully implicit scheme for the diffusion part. In addition, a rigorous analysis of convergence and stability of the Galerkin-characteristic method can be found in [6] in the framework of finite element discretizations. The paradigm one should keep in mind is that, in the Galerkin-characteristic finite element context, the interpolation consists of evaluating the solution at the characteristic curves using the nodal basis functions associated with the host element where the departure points are located. In the current work, we consider both the linear and quadratic basis functions on the host tetrahedron to calculate the solution at the characteristic curves.

Numerical results are presented for a linear advection-diffusion problem in a three-dimensional rotating velocity field and a transport problem in a well-developed pipeline flow. In the first case, analytical solution is available and thus it can be used to assess the accuracy of the proposed approach. In the other case, mesh convergence is shown to illustrate the ability of the Galerkin-characteristic finite element method to resolve transport problems in irregular domains subject to complex flows. Our method highly approximates numerical solution to these three-dimensional convection-diffusion problems. The obtained results demonstrate good front resolution without any oscillations near the areas with steep gradients or extensive numerical dissipation and without relying on very refined meshes. It should be mentioned that the main limitation of the Galerkin-characteristic finite element method in its current form remains the failure to conserve the mass for hyperbolic systems of conservation laws. In this case, correction terms and limiting procedures need to be accounted for in order to remedy this drawback. This paper is organized as follows. Formulation of the Galerkin-characteristic finite element method for three-dimensional convection-dominated problems is presented in section 2. The implementation of the method for the solution of convection-diffusion equations is also discussed in this section. In section 3, we examine the numerical performance of the proposed method using several test examples of convection-diffusion problems in three-dimensional domains. The proposed method is shown to enjoy the expected accuracy as well as the efficiency. Concluding remarks are summarized in section 4.

2 Three-dimensional Galerkin-characteristic finite element method

In this section we formulate the Galerkin-characteristic method in tetrahedral finite element framework for the numerical solution of the following three-dimensional convection-diffusion problem

$$\begin{aligned} \frac{\partial u}{\partial t} + \mathbf{v}(\mathbf{x},t)\cdot\nabla u - \nu\Delta u &= f(\mathbf{x},t), \qquad (\mathbf{x},t)\in\Omega\times(0,T], \\ u(\mathbf{x},0) &= u_0(\mathbf{x}), \qquad \mathbf{x}\in\Omega, \end{aligned} \tag{1}$$

where $\mathbf{x}=(x,y,z)^T$ is the position variable, $\nabla=(\frac{\partial}{\partial x},\frac{\partial}{\partial y},\frac{\partial}{\partial z})^T$ the gradient operator, Ω a spacial bounded domain in $\mathbb{R}^3$ with boundary $\partial\Omega$, and $(0,T]$ a time interval. Here, $u(\mathbf{x},t)$ denotes the concentration of some species, $\mathbf{v}(\mathbf{x},t)=(v_1(\mathbf{x},t),v_2(\mathbf{x},t),v_3(\mathbf{x},t))^T$ the velocity field assumed to be given either by measurements or by solving a flow problem such as Navier-Stokes equations. In (1), ν is the diffusion coefficient and $u_0(\mathbf{x})$ a given initial solution. Note that the convection-diffusion equations (1) have to be solved for the time interval $(0,T]$ in the spatial domain Ω equipped with given boundary and initial conditions. In practice, the boundary conditions are problem-dependent and their discussion is postponed for section 3 where numerical examples are discussed. For convection-diffusion equations, we also use the material derivative

$$\frac{Du}{Dt} = \frac{\partial u}{\partial t} + \mathbf{v}(\mathbf{x},t)\cdot\nabla u, \tag{2}$$

to model the convective term in (1). Note that the total derivative (2) measures the change rate of the function u following the trajectories of the flow particles.

To discretize the spatial domain Ω, we generate a quasi-uniform partition $\Omega_h\subset\Omega$ of small elements $\mathcal{T}_j$ that satisfy the following conditions:

(i) $\Omega_h = \bigcup_{j=1}^{Ne} \mathcal{T}_j$, where Ne is the number of elements in Ω_h.

(ii) If $\mathcal{T}_i$ and $\mathcal{T}_j$ are two different elements of Ω_h, then

$$\mathcal{T}_i \cap \mathcal{T}_j = \begin{cases} P_{ij}, & \text{a mesh point, or} \\ \Gamma_{ij}, & \text{a common face, or} \\ \partial\Gamma_{ij}, & \text{a common edge, or} \\ \emptyset, & \text{empty set.} \end{cases}$$

(iii) There exists a positive constant k such that for all $j \in \{1, \ldots, Ne\}$, $\frac{R_j}{h_j} > k$ ($h_j \leq h$), where R_j is the radius of the sphere inscribed in $\mathcal{T}_j$, and h_j is the largest edge of $\mathcal{T}_j$.

The conforming finite element space for the solution that we use is defined as

$$V_h = \Big\{ C_h \in \mathcal{C}^0(\Omega) : \quad C_h\big|_{\mathcal{T}_j} \in P(\mathcal{T}_j), \quad \forall\ \mathcal{T}_j \in \Omega_h \Big\}, \tag{3}$$

with

$$P(\mathcal{T}_j) = \Big\{ p(\mathbf{x}) : \quad p(\mathbf{x}) = \hat{p} \circ F_j^{-1}(\mathbf{x}), \quad \hat{p} \in P_m(\hat{\mathcal{T}}) \Big\},$$

where $\hat{p}(\mathbf{x})$ is a polynomial of degree $\leq m$ defined on the element $\hat{\mathcal{T}}_j$ and $P_m(\hat{\mathcal{T}})$ is the set of polynomials of degree $\leq m$ defined on the reference element $\hat{\mathcal{T}}$. Here, $F_j : \hat{\mathcal{T}} \longrightarrow \mathcal{T}_j$ is an invertible one-to-one mapping between physical and reference elements.

For the time discretization, we divide the time interval into N subintervals $[t_n, t_{n+1}]$ with length $\Delta t = t_{n+1} - t_n$ for $n = 0, 1, \ldots, N$. We also use the notation w^n to denote the value of a generic function w at time t_n. Hence, we formulate the finite element solution to $u^n(\mathbf{x})$ as

$$u_h^n(\mathbf{x}) = \sum_{j=1}^{M} U_j^n \phi_j(\mathbf{x}), \tag{4}$$

where M is the number of solution mesh points in the partition Ω_h. Here, the functions U_j^n are the corresponding nodal values of $u_h^n(\mathbf{x})$ defined as $U_j^n = u_h^n(\mathbf{x}_j)$ where $\{\mathbf{x}_j\}_{j=1}^M$ are the set of solution mesh points in the partition Ω_h. In (4), $\{\phi_j\}_{j=1}^M$ are the set of global nodal basis functions of V_h characterized by the property $\phi_i(\mathbf{x}_j) = \delta_{ij}$ with δ_{ij} denoting the Kronecker symbol. We introduce $\{\mathbf{x}_1, \ldots, \mathbf{x}_N\}$ the set of N node points in the element $\mathcal{T}_j$. We also define $\{\varphi_j\}_{j=1}^N$ the set of local basis functions for $\mathcal{T}_j$ in V_h characterized by the property $\varphi_i(\mathbf{x}_j) = \delta_{ij}$. Hereafter, unless otherwise stated, the subscripts h and j are used to refer to coefficients associated with the whole mesh Ω_h and a mesh element $\mathcal{T}_j$, respectively. Notice that the set $\{\varphi_j\}_{j=1}^N$ is a local restriction on the element $\mathcal{T}_j$ of the set of the global basis functions $\{\phi_j\}_{j=1}^M$.

2.1 Approximation of characteristic curves

The modified method of characteristics aims to impose a regular grid at the new time level and to backtrack the flow trajectories to the previous time level. At the old time level, the required variables are evaluated by interpolation from their known values on a regular grid. Following for example [16, 5], the characteristic curves associated with the equation (2) are the solution of the initial value problem

$$\begin{aligned} \frac{d\mathbf{X}_h(t;\mathbf{x}_h)}{dt} &= \mathbf{v}\big(\mathbf{X}_h(t;\mathbf{x}_h), t\big), \quad t \in [t_n, t_{n+1}], \\ \mathbf{X}_h(t_{n+1};\mathbf{x}_h) &= \mathbf{x}_h. \end{aligned} \tag{5}$$

Note that $\mathbf{X}_h(t;\mathbf{x}_h) = \big(X_h(t;\mathbf{x}_h), Y_h(t;\mathbf{x}_h), Z_h(t;\mathbf{x}_h)\big)^T$ is the departure point at time t of a particle that will arrive in $\mathbf{x}_h = \big(x_h, y_h, z_h\big)^T$ at time t_{n+1}. In general, the Galerkin-characteristic method does not follow the flow particles forward in time, as the Lagrangian method does, instead it traces backwards the position at time t_n of particles that will reach the points of a fixed mesh at time t_{n+1}. Therefore, the Galerkin-characteristic method avoids the grid distortion difficulties that the conventional Lagrangian schemes have. The solutions of ordinary differential equations (5) can be expressed as

$$\mathbf{X}_h(t_n;\mathbf{x}_h) = \mathbf{x}_h - \int_{t_n}^{t_{n+1}} \mathbf{v}\left(\mathbf{X}_h(t;\mathbf{x}_h), t\right)\, dt. \tag{6}$$

To evaluate the integral in (6), we use a second-order extrapolation based on the mid-point rule used in the context of semi-Lagrangian schemes to integrate the weather prediction problems in [23]. Hence, we use $\mathbf{d}_h$ to denote the displacement between a mesh point $\mathbf{x}_h$ on the new level and the departure point $\mathbf{X}_h(t_n;\mathbf{x})$ of the trajectory to this point on the previous time level *i.e.*

$$\mathbf{d}_h = \mathbf{x}_h - \mathbf{X}_h(t_n;\mathbf{x}_h). \tag{7}$$

Applying the mid-point rule to approximate the integral in (6) yields

$$\mathbf{d}_h = \Delta t \mathbf{v}_h\left(\mathbf{X}_h(t_{n+\frac{1}{2}};\mathbf{x}_h), t_{n+\frac{1}{2}}\right).$$

Using the second-order extrapolation

$$\mathbf{v}_h\left(\mathbf{x}_h, t_{n+\frac{1}{2}}\right) = \frac{3}{2}\mathbf{v}_h\left(\mathbf{x}_h, t_n\right) - \frac{1}{2}\mathbf{v}_h\left(\mathbf{x}_h, t_{n-1}\right),$$

and the second-order approximation

$$\mathbf{X}_h(t_{n+\frac{1}{2}};\mathbf{x}_h) = \mathbf{x}_h - \frac{1}{2}\mathbf{d}_h,$$

we obtain the following implicit formula for $\mathbf{d}_h$

$$\mathbf{d}_h = \Delta t\left(\frac{3}{2}\mathbf{v}_h\left(\mathbf{x}_h - \frac{1}{2}\mathbf{d}_h, t_n\right) - \frac{1}{2}\mathbf{v}_h\left(\mathbf{x}_h - \frac{1}{2}\mathbf{d}_h, t_{n-1}\right)\right).$$

To compute $\mathbf{d}_h$ we consider the following successive iteration procedure:

$$\begin{aligned}
\mathbf{d}_h^{(0)} &= \Delta t\left(\frac{3}{2}\mathbf{v}_h\left(\mathbf{x}_h, t_n\right) - \frac{1}{2}\mathbf{v}_h\left(\mathbf{x}_h, t_{n-1}\right)\right), \\
\mathbf{d}_h^{(k)} &= \Delta t\left(\frac{3}{2}\mathbf{v}_h\left(\mathbf{x}_h - \frac{1}{2}\mathbf{d}_h^{(k-1)}, t_n\right) - \frac{1}{2}\mathbf{v}_h\left(\mathbf{x}_h - \frac{1}{2}\mathbf{d}_h^{(k-1)}, t_{n-1}\right)\right), \quad k = 1, 2, \ldots.
\end{aligned} \tag{8}$$

The iterations (8) are terminated when the following criteria

$$\frac{\left\|\mathbf{d}^{(k)} - \mathbf{d}^{(k-1)}\right\|}{\left\|\mathbf{d}^{(k-1)}\right\|} < \varepsilon, \tag{9}$$

is satisfied for the Euclidean norm $\|\cdot\|$ and a given tolerance ε. In our computational test examples, the iterations in (8) were continued until the trajectory changed by less than 10^{-7}. However, in practice it is not recommended to repeat the iteration process more than few times due to efficiency considerations. Once an approximation of the displacement $\mathbf{d}_h$ is achieved in (8), the characteristic curves are obtained for each gridpoint from (7) as

$$\mathbf{X}_h(t_n;\mathbf{x}_h) = \mathbf{x}_h - \mathbf{d}_h.$$

In general the departure points $\mathbf{X}_h(t_n;\mathbf{x}_h)$ do not coincide with the spatial position of a gridpoint. A requirement is then that the scheme to compute $\mathbf{X}_h(t_n;\mathbf{x}_h)$ be equipped with a search-locate algorithm to find the host element where such point is located. To perform this step in our computations, we have implemented a search-locate algorithm especially designed in [1] for the semi-Lagrangian method that works for triangles, quadrilaterals, tetrahedra, and hexahedra elements in unstructured discretizations. Since the departure point $\mathbf{X}_h(t;\mathbf{x}_h)$ would not lie on a mesh point, the solution field at the characteristic feet must be obtained by interpolation from known values at the gridpoints of the element where $\mathbf{X}_h(t;\mathbf{x}_h)$ belongs. Here, the Lagrangian interpolation is performed in the host element of departure points using the finite element basis functions. Therefore, an advantage of the finite element method is that it can employ a high-order basis functions and there is no need for constructing explicitly interpolation polynomials as usually carried out in the finite difference discretizations, compare the references [18, 15, 20] among others. Thus, the finite element solution to $\widetilde{u}_h^n = u\left(\mathbf{X}_h(t_n;\mathbf{x}_h), t_n\right)$ is approximated by

$$\widetilde{u}_h^n = \sum_{j=1}^{M} \widetilde{U}_j^n \phi_j, \tag{10}$$

where $\widetilde{U}_j^n$ are evaluated by finite element interpolation of $u_h^n(\mathbf{x})$ at the feet of characteristic curves $\mathbf{X}_h(t_n;\mathbf{x}_h)$. Note that, this procedure needs less computational work than using a piecewise exact method for projecting the information from the background Eulerian grid onto the Lagrangian grid as those reported in [5, 14] for two-dimensional problems.

2.2 Implementation for convection-diffusion problems

In the current study, to deal with the diffusive part in the equations (1) we consider the second-order Crank-Nicolson integration method along the characteristics. Thus, assuming the solution u_h is approximated by the characteristic method, then the weak formulation reads

$$\left(\frac{Du}{Dt}, v_h\right) - \left(\nu\Delta u_h, v_h\right) = \left(f_h, v_h\right), \qquad \forall\, v_h \in W_h, \tag{11}$$

where

$$W_h = \left\{ u_h \in V_h : \quad \nu\frac{\partial u_h}{\partial n}\bigg|_{\partial\Omega} = 0 \right\}.$$

By virtue of definitions of the finite element operators given above, it follows that (11) reduces to a system of ordinary differential equations as

$$[\mathbf{M}]\,\frac{D\mathbf{U}}{Dt} + [\mathbf{S}]\,\mathbf{U} = [\mathbf{M}]\,\mathbf{F}, \qquad t \in [t_n, t_{n+1}], \tag{12}$$

where $\widetilde{\mathbf{U}}^n$ known as initial condition at t_n. In (12), $\mathbf{U} = (U_1, \ldots, U_M)^T$, $[\mathbf{M}]$ and $[\mathbf{S}]$ are sparse symmetric matrices the elements of which are given by

$$m_{ij} = \int_\Omega \phi_i\phi_j \, d\mathbf{x}, \qquad i,j = 1,2\ldots,M,$$

and

$$s_{ij} = \int_\Omega \nu\nabla\phi_i\nabla\phi_j \, d\mathbf{x}, \qquad i,j = 1,2\ldots,M,$$

respectively. Applied to the semi-discrete equations (12), the Crank-Nicolson scheme yields

$$[\mathbf{M}]\,\frac{\mathbf{U}^{n+1} - \widetilde{\mathbf{U}}^n}{\Delta t} + \frac{1}{2}\,[\mathbf{S}]\,\mathbf{U}^{n+1} + \frac{1}{2}\,[\mathbf{S}]\,\widetilde{\mathbf{U}}^n = \frac{1}{2}\,[\mathbf{M}]\,\mathbf{F}^{n+1} + \frac{1}{2}\,[\mathbf{M}]\,\widetilde{\mathbf{F}}^n, \tag{13}$$

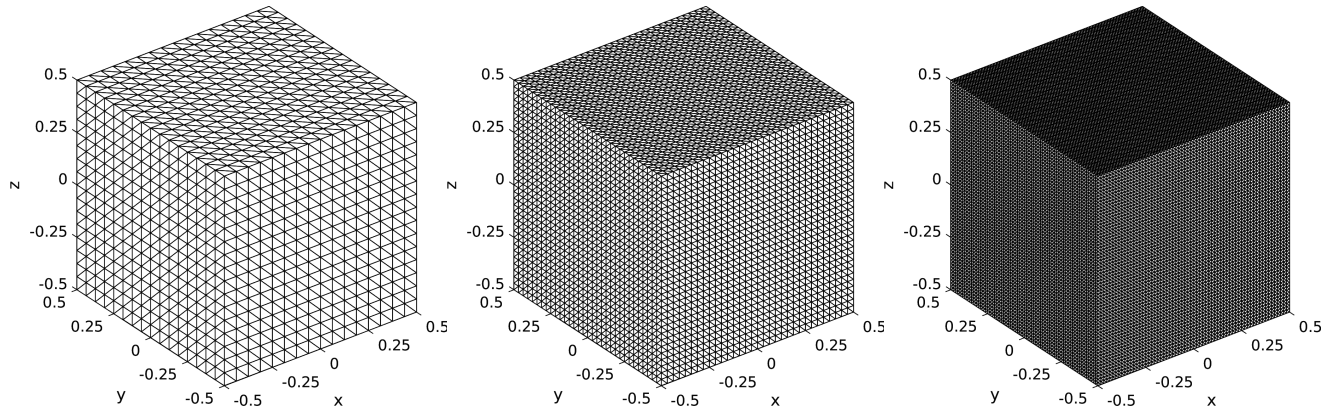

Figure 1: Uniform meshes with spatial steps $h = \frac{1}{32}$ (left), $\frac{1}{64}$ (middle) and $\frac{1}{128}$ (right) used in our simulations for advection-diffusion problems in circular and elliptical flow fields.

where all the terms with tilde are evaluated at the departure point $\mathbf{X}(t_n; \mathbf{x})$. Note that the considered method requires solution of uncoupled elliptic problems such that their finite element discretization leads to well-conditioned linear systems of algebraic equations for which, very efficient solvers can be implemented. Therefore, by taking advantage of these properties we solve the linear systems in (13) by the conjugate gradient solver using an incomplete Cholesky factorization. This yields to an efficient method for solving this class of linear systems of algebraic equations, compare for example [7].

3 Numerical results

In this section we present numerical results for several examples to demonstrate the performance of the proposed Galerkin-characteristic finite element method. For the first class of examples, analytical solutions are readily available which makes it ideal for a quantitative as well as qualitative validation of the proposed method. We compare numerical results obtained using the linear P_1 and quadratic P_2 finite elements for these examples. We also present numerical results for a transport problem in pipeline flows. The objective of this test example is to illustrate that, using reasonably large time steps, the Galerkin-characteristic finite element method reproduces the corresponding transport patterns and it accurately captures the flow structures with very little numerical diffusion even after long time simulations. Here, we define the CFL number associated to the equations (1) as

$$\mathrm{CFL} = \sqrt{\mathrm{CFL}_x^2 + \mathrm{CFL}_y^2 + \mathrm{CFL}_z^2}, \tag{14}$$

where

$$\mathrm{CFL}_x = \max_{x,y,z} |v_1| \frac{\Delta t}{h}, \qquad \mathrm{CFL}_y = \max_{x,y,z} |v_2| \frac{\Delta t}{h}, \qquad \mathrm{CFL}_z = \max_{x,y,z} |v_3| \frac{\Delta t}{h}.$$

Notice that to reduce the computational cost, the timesteps Δt are chosen as large as possible. This makes most explicit Eulerian-based finite element methods noncompetitive, since they are subject to stability restriction conditions. Therefore, the criteria of choosing time steps in our algorithm was mainly based on accuracy considerations. Practically, we take the spatial step h proportional to the time step Δt, so the error decreases quadratically in both h and Δt. In order to obtain convergence at a quadratic rate, it is only needed that $h/\Delta t$ is bounded above. In other words, our proposed method is unconditionally stable with no need to satisfy a CFL-type condition. All the computations were performed on a Pentium PC with one processor of 2.2 GB of RAM and 1.8 GHz using serial Fortran compiler.

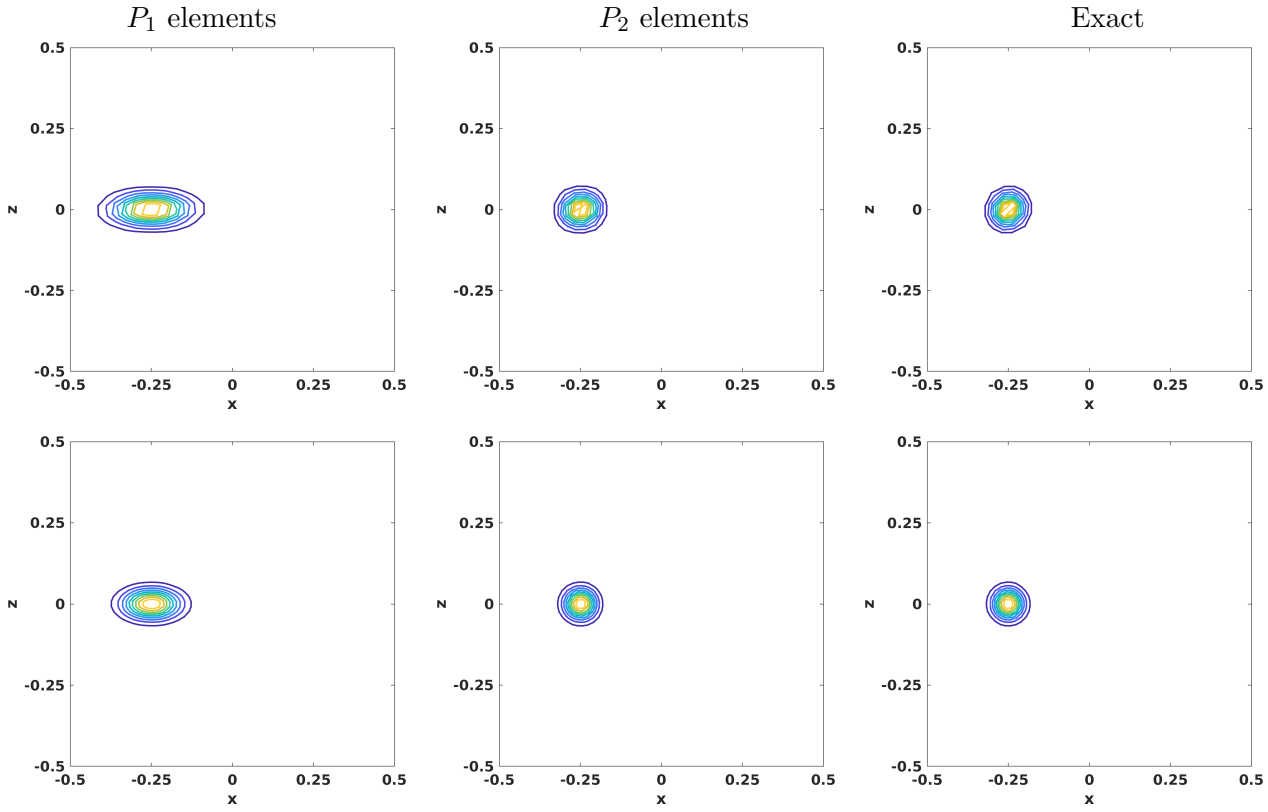

Figure 2: Contours of the solution in the x-z plane at $y = 0$ for pure advection of rotating the Gaussian sphere after 2 revolutions using CFL = 10 and meshes with $h = \frac{1}{64}$ (first row) and $h = \frac{1}{128}$ (second row).

3.1 Rotating a Gaussian sphere in circular flow fields

We consider the advection-diffusion problem of rotating a Gaussian sphere in circular three-dimensional flow fields. The two-dimensional version of this example has been extensively used in the literature to test the accuracy of transport methods, see for example [16, 21]. The equations are of the form (1) with $\mathbf{v} = (-\omega y, \omega x, 0)^T$. Initial and boundary conditions are taken from the analytical solution

$$u(x, y, z, t) = \frac{\sigma^2}{\sigma^2 + \omega\nu t} \exp\left(-\frac{(\bar{x} - x_0)^2 + (\bar{y} - y_0)^2 + (z - z_0)^2}{\sigma^2 + \omega\nu t}\right),$$

where $\bar{x} = x\cos(\omega t) + y\sin(\omega t)$, $\bar{y} = -x\sin(\omega t) + y\cos(\omega t)$, $x_0 = -0.25$, $y_0 = 0$ and $\sigma^2 = 0.002$. The computational domain is the unit cube $[-\frac{1}{2}, \frac{1}{2}] \times [-\frac{1}{2}, \frac{1}{2}] \times [-\frac{1}{2}, \frac{1}{2}]$ and the time period required for one complete rotation is $\frac{\pi}{2}$. In all our simulations for this test example, we use uniform meshes with spatial steps $h = \frac{1}{32}$, $\frac{1}{64}$ and $\frac{1}{128}$ as shown in Figure 1. From the definition (14), the CFL number associated to this example is $\omega\frac{\sqrt{2}}{2}\frac{\Delta t}{h}$ and it is set to different values in our simulations.

In Figure 2 we illustrate 10 equi-distributed contourlines of the cross-section solutions in the x-z plane at $y = 0$ obtained using P_1 and P_2 elements after 1 revolution using a CFL = 10 and two structured meshes with $h = \frac{1}{64}$ and $h = \frac{1}{128}$. For a comparison reason, we have also included analytical solutions in this figure. It is evident that the solutions obtained using P_2 elements are more accurate than those obtained using the P_1 elements for both meshes considered. The one-dimensional plots in Figure 3 and Figure 4 correspond to cross-section solutions at $y = z = 0$ of the results obtained after 1 and 2 revolutions, respectively. We consider three different CFL numbers in this case namely, CFL = 2.5, 5 and 10. A visual comparison of the results in these figures shows severe numerical dissipation in the

Table 1: Results for pure advection of rotating the Gaussian sphere after 1 and 2 revolutions using different meshes and values of CFL. The analytical maximum is 1 and the CPU times are given in seconds.

After 1 revolution

		P_1 elements			P_2 elements		
CFL	h	Max	L^1-error	CPU	Max	L^1-error	CPU
2.5	$\frac{1}{32}$	0.041340	7.302728E-04	0.032	0.385970	4.008634E-04	0.269
	$\frac{1}{64}$	0.149291	5.856856E-04	0.237	0.833229	7.841065E-05	2.149
	$\frac{1}{128}$	0.440721	2.966778E-04	2.091	0.986686	6.424644E-06	17.071
5	$\frac{1}{32}$	0.089497	7.073935E-04	0.014	0.561956	2.592411E-04	0.138
	$\frac{1}{64}$	0.276455	4.458083E-04	0.127	0.887428	4.158871E-05	1.092
	$\frac{1}{128}$	0.604019	1.806305E-04	1.090	0.990603	3.842980E-06	9.043
10	$\frac{1}{32}$	0.220604	5.739867E-04	0.008	0.601914	1.856439E-04	0.067
	$\frac{1}{64}$	0.425191	3.058723E-04	0.065	0.944249	2.421203E-05	0.546
	$\frac{1}{128}$	0.746478	1.021212E-04	0.558	0.994381	2.302662E-06	4.499

After 2 revolutions

		P_1 elements			P_2 elements		
CFL	h	Max	L^1-error	CPU	Max	L^1-error	CPU
2.5	$\frac{1}{32}$	0.018815	7.003067E-04	0.062	0.290810	5.099891E-04	0.526
	$\frac{1}{64}$	0.083973	6.945126E-04	0.471	0.756841	1.304702E-04	4.152
	$\frac{1}{128}$	0.282445	4.374713E-04	4.089	0.973744	1.187163E-05	33.891
5	$\frac{1}{32}$	0.046456	7.338695E-04	0.028	0.463282	3.724758E-04	0.268
	$\frac{1}{64}$	0.167037	5.792228E-04	0.267	0.844775	6.649892E-05	2.170
	$\frac{1}{128}$	0.434056	2.978817E-04	2.245	0.984570	6.565027E-06	17.671
10	$\frac{1}{32}$	0.107079	7.015479E-04	0.015	0.547961	2.631193E-04	0.141
	$\frac{1}{64}$	0.285538	4.403378E-04	0.128	0.912359	4.084245E-05	1.109
	$\frac{1}{128}$	0.590172	1.805293E-04	1.131	0.991105	3.863595E-06	9.091

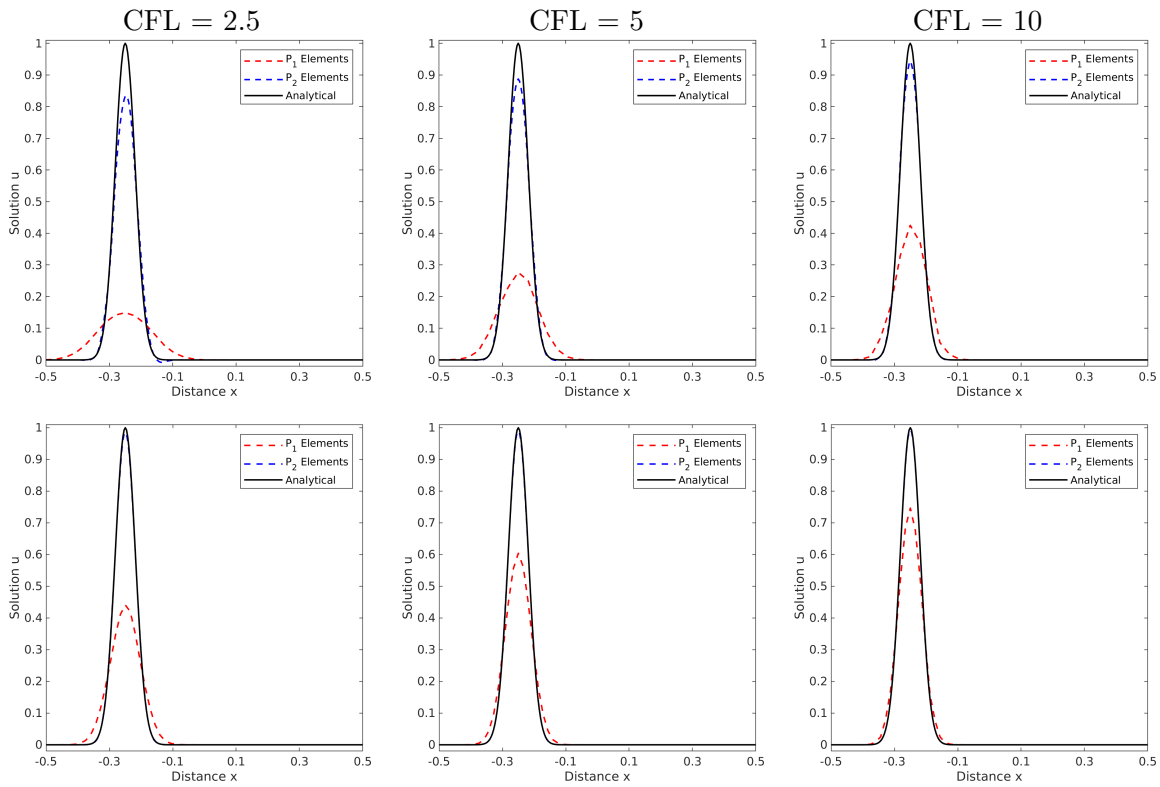

Figure 3: Cross-sections of the solution at $y = z = 0$ for pure advection of rotating the Gaussian sphere after 1 revolution using different values of CFL numbers and meshes with $h = \frac{1}{64}$ (first row) and $h = \frac{1}{128}$ (second row).

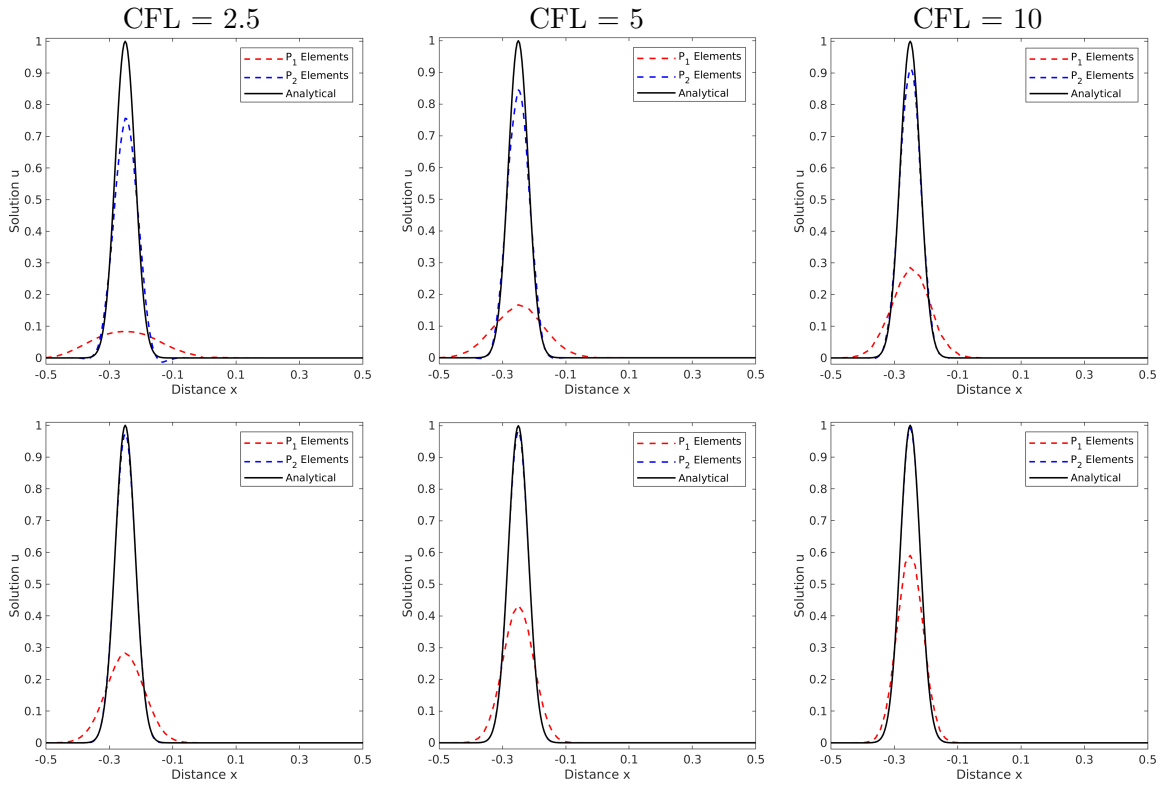

Figure 4: Same as Figure 3 but after 2 revolutions.

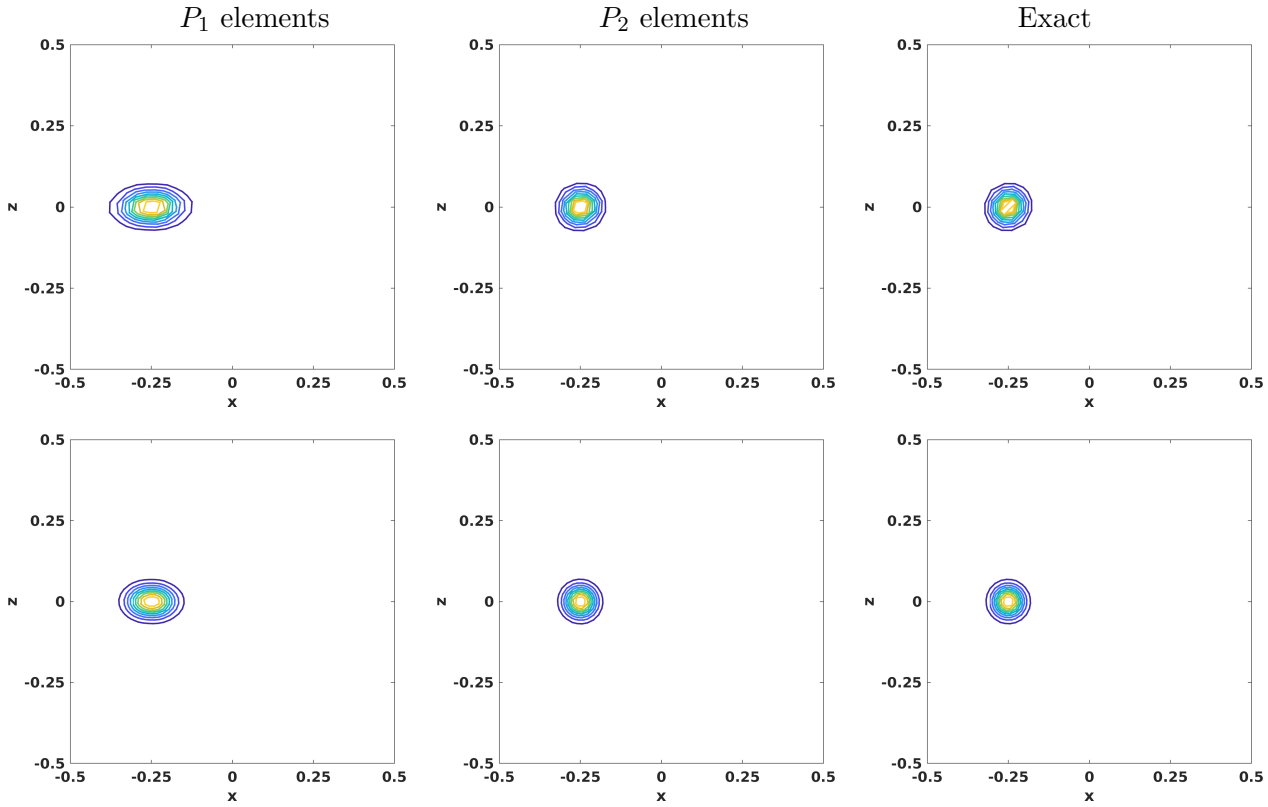

Figure 5: Contours of the solution in the x-z plane at $y = 0$ for advection-diffusion of rotating the Gaussian sphere after 2 revolutions using $\nu = 10^{-5}$, CFL = 10 and meshes with $h = \frac{1}{64}$ (first row) and $h = \frac{1}{128}$ (second row).

P_1 solutions. This numerical dissipation is more pronounced for small values of CFL and it reduces as the mesh is refined. For a mesh with $h = \frac{1}{64}$ and after 2 revolutions, the the solutions obtained using P_1 elements exhibit substantially large diffusion, specially at the feet of the Gaussian pulse where the gradient is sharp. From the same figures we observe an absence of this numerical dissipation in the P_2 results. Note that the accuracy in the proposed Galerkin-characteristic finite element method improves as the value of CFL increases, compare the results obtained using CFL = 2.5 and CFL = 10 in Figure 3 and Figure 4. It is clear that the Galerkin-characteristic finite element method using P_2 elements performs best for this test example.

A quantitative comparison of the results computed using P_1 and P_2 elements for different values of CFL numbers and meshes is summarized in Table 1. We report the L^1-error, the maximum (Max) values of the computed solutions, and the CPU times given in seconds. We present numerical results after 1 and 2 revolutions using different meshes and CFL numbers. In terms of the considered error, the P_2 results are more accurate than the results obtained using the P_1 elements for all the CFL numbers considered. From the values of Max in Table 1 we observe very low values for the P_1 results compared to those obtained using the P_2 elements. After 2 rotations, the Galerkin-characteristic finite element method using P_1 yields large values of the L^1-error and low values for the maximum of the computed solutions for the considered transport conditions. It is also evident that the CPU times of the P_2 elements are larger than the CPU time of the P_1 elements. For the considered adevction conditions with CFL = 10, the CPU time of the quadratic P_2 elements is about nine times larger than the CPU time of the linear P_1 elements.

Next we include the physical diffusion in the problem by solving the advection-diffusion equation (1) with two diffusion coefficients $\nu = 10^{-6}$ and $\nu = 10^{-5}$. The obtained results for $\nu = 10^{-5}$ using the P_1

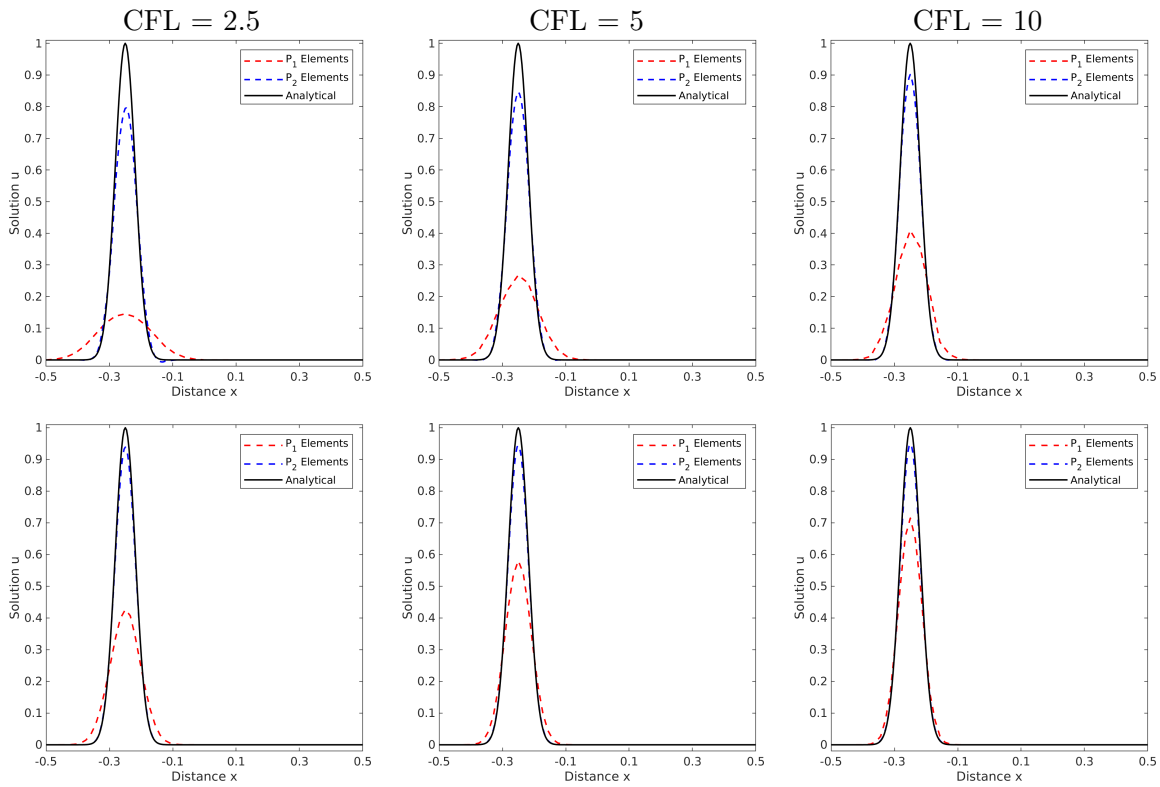

Figure 6: Cross-sections of the solution at $y = z = 0$ for advection-diffusion of rotating the Gaussian sphere after 1 revolution using $\nu = 10^{-5}$, different values of CFL and meshes with $h = \frac{1}{64}$ (first row) and $h = \frac{1}{128}$ (second row).

and P_2 elements along with exact solutions are presented in Figure 5 for 10 equi-distributed contourlines of the cross-section solutions in the x-z plane at $y = 0$ after 2 revolution using a CFL $= 10$ and two meshes with $h = \frac{1}{64}$ and $h = \frac{1}{128}$. Figure 6 shows the cross-section solutions at $y = z = 0$ of the results obtained after 2 revolutions. As in the previous simulations, it is clear from the results presented that the numerical diffusion is more pronounced in the results obtained using the P_1 elements, compare the two-dimensional contours in Figure 5 and the one-dimensional cross-sections in Figure 6. Again the Galerkin-characteristic finite element method using P_2 elements performs best for this test example of advection-diffusion problems.

To quantify the comparison between the results computed using P_1 and P_2 elements, the L^1 errors, maximum values of the computed solutions and the CPU times are presented in Table 2 for $\nu = 10^{-6}$ and $\nu = 10^{-5}$. We present numerical results after 1 revolution using different meshes and values of CFL. In terms of the L^1 errors, the P_2 results are more accurate than the results obtained using the P_1 elements for both diffusion coefficients considered. From the values of Max in Table 2 for $\nu = 10^{-6}$ and $\nu = 10^{-5}$ we observe low values for the P_1 results that are substantially improved in the P_2 results. Concerning the computational cost, the CPU times of the P_2 elements are larger than the CPU time of the P_1 elements. Note that timings, in seconds, include all aspects of computations (grid generation, search-locate procedure, reconstruction of matrices and solution of linear systems). It is to be remarked that, the Galerkin-characteristic finite element method is typically built to solve this class of convection-dominated advection-diffusion problems using times steps ten to twenty times larger than its Eulerian counterparts.

Table 2: Results for advection-diffusion of rotating the Gaussian sphere for two diffusion coefficients $\nu = 10^{-5}$ and $\nu = 10^{-6}$ after 1 revolutions using different meshes and values of CFL. The analytical maximum for $\nu = 10^{-5}$ and $\nu = 10^{-6}$ are 0.969540 and 0.996868, respectively. The CPU times are given in seconds.

$\nu = 10^{-5}$

		P_1 elements			P_2 elements		
CFL	h	Max	L^1-error	CPU	Max	L^1-error	CPU
2.5	$\frac{1}{32}$	0.040616	7.260997E-04	0.311	0.373080	4.005624E-04	0.591
	$\frac{1}{64}$	0.145579	5.835766E-04	1.069	0.794779	7.552244E-05	7.219
	$\frac{1}{128}$	0.426542	2.947165E-04	5.998	0.938866	8.405223E-06	37.014
5	$\frac{1}{32}$	0.087743	7.079410E-04	0.145	0.539201	2.587153E-04	0.241
	$\frac{1}{64}$	0.267674	4.413862E-04	0.531	0.846346	4.080042E-05	3.312
	$\frac{1}{128}$	0.580847	1.811738E-04	3.311	0.945034	7.950874E-06	18.911
10	$\frac{1}{32}$	0.213674	5.670267E-04	0.017	0.577416	1.870931E-04	0.113
	$\frac{1}{64}$	0.409034	3.044726E-04	0.272	0.901420	2.354583E-05	1.613
	$\frac{1}{128}$	0.714854	1.037857E-04	1.679	0.950017	7.745346E-06	9.409

$\nu = 10^{-6}$

		P_1 elements			P_2 elements		
CFL	h	Max	L^1-error	CPU	Max	L^1-error	CPU
2.5	$\frac{1}{32}$	0.219893	5.728901E-04	0.191	0.384640	4.019564E-04	1.010
	$\frac{1}{64}$	0.148908	5.053470E-04	1.517	0.829107	7.808369E-05	7.141
	$\frac{1}{128}$	0.439262	2.964940E-04	9.231	0.981404	6.303629E-06	49.981
5	$\frac{1}{32}$	0.089316	7.068638E-04	0.051	0.559582	2.605622E-04	0.461
	$\frac{1}{64}$	0.275546	4.453763E-04	0.731	0.883068	4.142742E-05	3.138
	$\frac{1}{128}$	0.601621	1.807011E-04	4.819	0.985718	3.825651E-06	25.411
10	$\frac{1}{32}$	0.041256	7.256858E-04	0.026	0.599351	1.869357E-04	0.151
	$\frac{1}{64}$	0.423516	3.057508E-04	0.342	0.939765	2.401774E-05	1.951
	$\frac{1}{128}$	0.743204	1.022450E-04	2.330	0.989836	2.270755E-06	12.719

3.2 Rotating a pulse in elliptical flow fields

In this example we consider a fully three-dimensional advection problem of rotating a pulse in oblique flow fields proposed in [2]. The governing equations are given by (1) where the velocity is defined as $\mathbf{u} = (-\omega y, \omega x, (x+y)/2)^T$ with $\nu = 0$ and $\omega = 4$. Initial and boundary conditions are derived from the analytical solution

$$u(x,y,z,t) = \begin{cases} \dfrac{(1+\cos(\omega\pi r))^2}{4}, & \text{if} \quad r < \dfrac{1}{\omega}, \\ 0, & \text{if} \quad r \geq \dfrac{1}{\omega}, \end{cases}$$

where $r = \sqrt{(\bar{x}-x_0)^2 + (\bar{y}-y_0)^2 + (\bar{z}-z_0)^2}$ with $x_0 = -0.25$, $y_0 = 0$, $z_0 = 0.25$, $\bar{x} = x\cos(\omega t) + y\sin(\omega t)$, $\bar{y} = -x\sin(\omega t) + y\cos(\omega t)$ and $\bar{z} = z - (\bar{x} - x + \bar{y} - y)/2$. The computational domain is the unit cube $\Omega = [-0.5, 0.5]^3$ covered by different uniform meshes and the time period required for one complete

oblique rotation is $\frac{\pi}{2}$. As in the previous example, we present results for different values of CFL and the time steps used in the simulations are calculated using the definition (14).

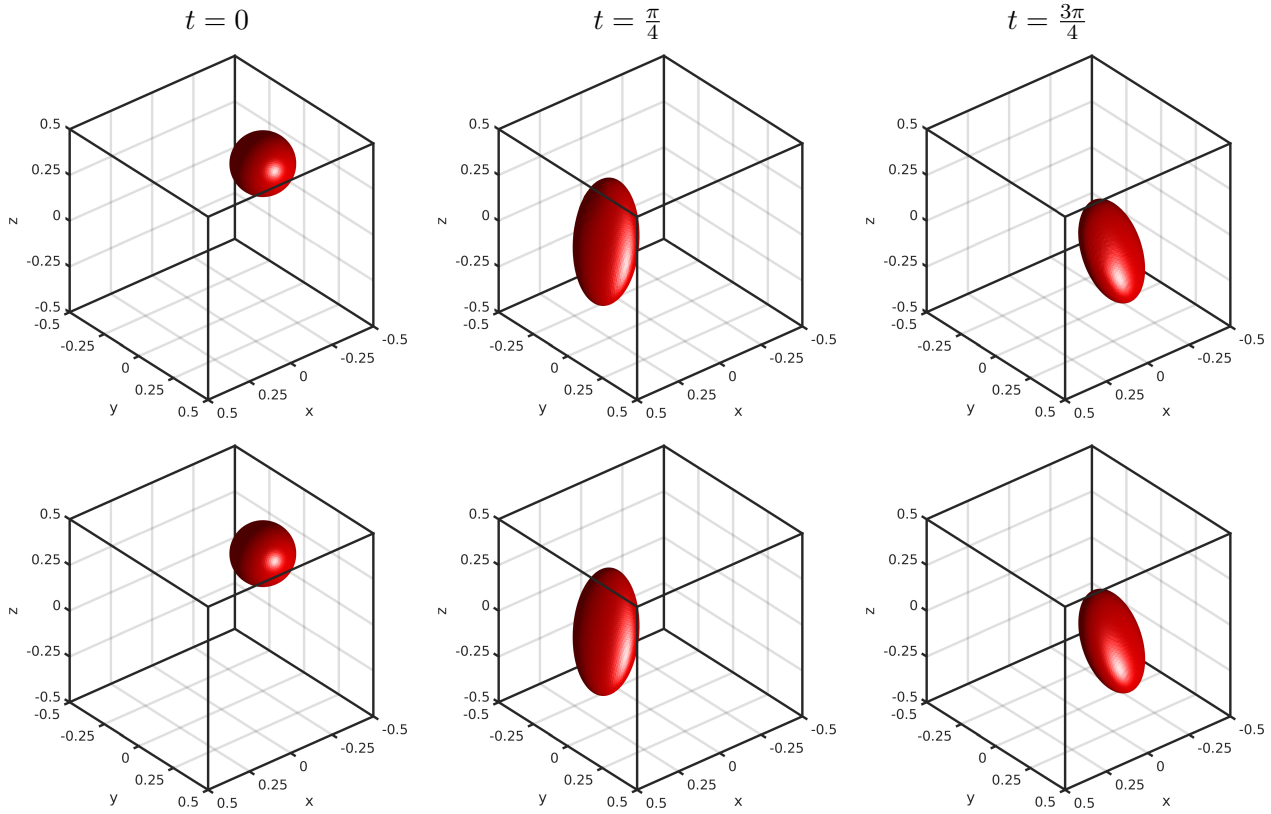

Figure 7: Numerical iso-surfaces (first row) and analytical results (second row) for rotating a pulse in elliptical flow fields at three different times using $h = \frac{1}{64}$ and CFL =10.

In Figure 7 we display the iso-surfaces of the initial solution and the computed solutions at two different times, $t = \frac{\pi}{4}$ and $\frac{3\pi}{4}$ using a mesh with P_2 elements and $h = \frac{1}{64}$. For comparison, analytical solutions are also included in this figure. It is clear that the Galerkin-characteristic finite element method accurately captures the expected transport and its propagation along the elliptical trajectory. Figure 8 and Figure 9 exhibit 10 equi-distributed contourlines of the cross-section solutions in the x-z plane at $y = 0$ after 1 and 2 revolutions, respectively. We present analytical and computational results using P_1 and P_2 elements with CFL = 10 and two meshes with $h = \frac{1}{64}$ and $h = \frac{1}{128}$. As expected, the numerical results obtained using P_1 elements are more diffusive than those computed using P_2 elements. To further visualize this effect we display in Figure 10 and Figure 11 the cross-section along the horizontal line at $y = z = 0$ for the results using three different values of CFL = 2.5, 5 and 10. It is clear that the transport resolution and location are deteriorated with the excessive dissipation included by the P_1 elements. On the other hand, the P_2 solutions are free of excessive numerical diffusion and the transport is well resolved without requiring fine meshes or small time steps.

Now we turn our attention to a quantitative comparison of the results computed using P_1 and P_2 elements for different values of CFL and mesh densities. In Table 3 we list the L^1-error, the maximum (Max) values of the computed solutions, and the CPU times for results computed using P_1 and P_2 elements for different values of CFL and meshes after 1 and 2 revolutions. Under the considered transport conditions, the results obtained using the P_2 elements are more accurate than the results obtained using the P_1 elements for both 1 and 2 revolutions. Notice that low values of Max have been detected in the P_1 solutions compared to those obtained for the P_2 solutions. Refining the mesh or increasing the CFL numbers yield improvements in the results obtained for the L^1-error and maximum values of the computed

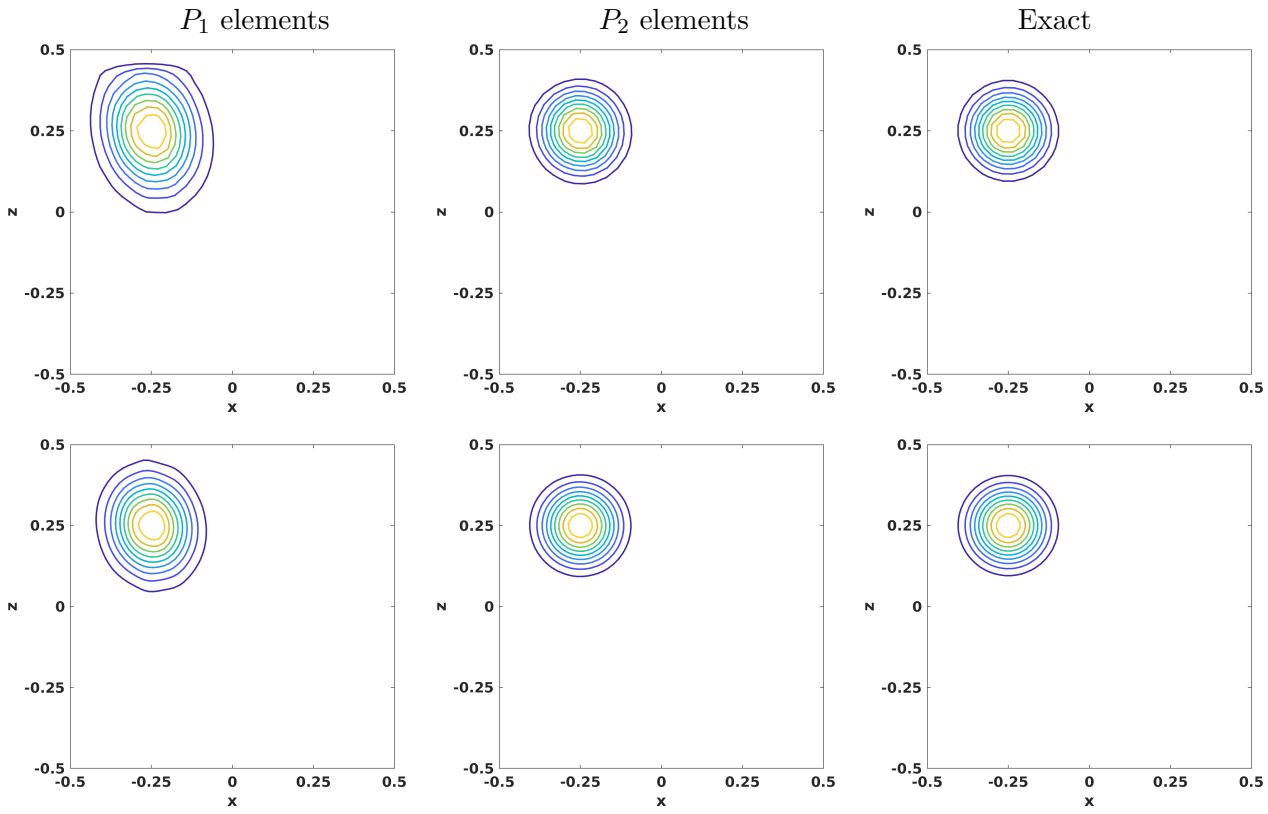

Figure 8: Contours of the solution in the x-z plane at $y = 0$ for a pulse in elliptical flow fields after 1 revolution using CFL $= 10$ and meshes with $h = \frac{1}{64}$ (first row) and $h = \frac{1}{128}$ (second row).

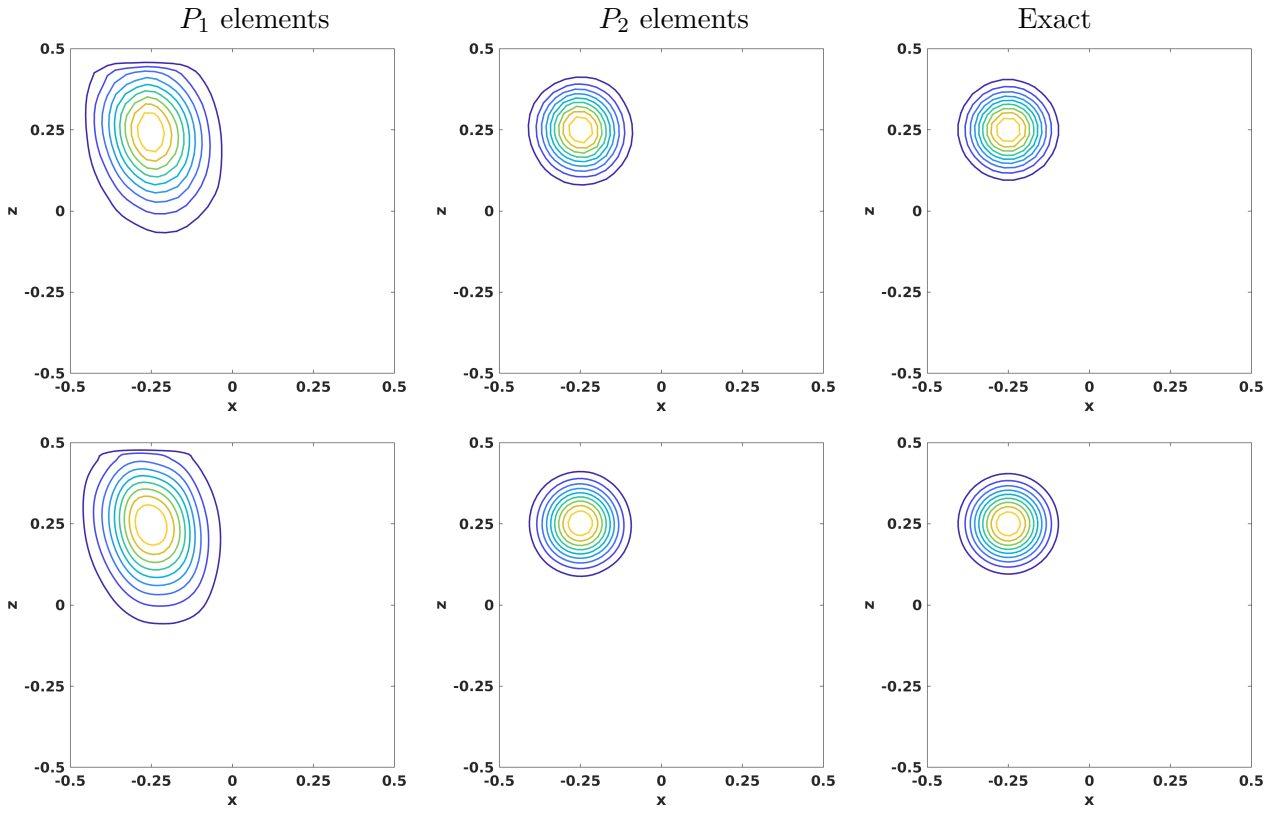

Figure 9: Same as Figure 8 but after 2 revolutions.

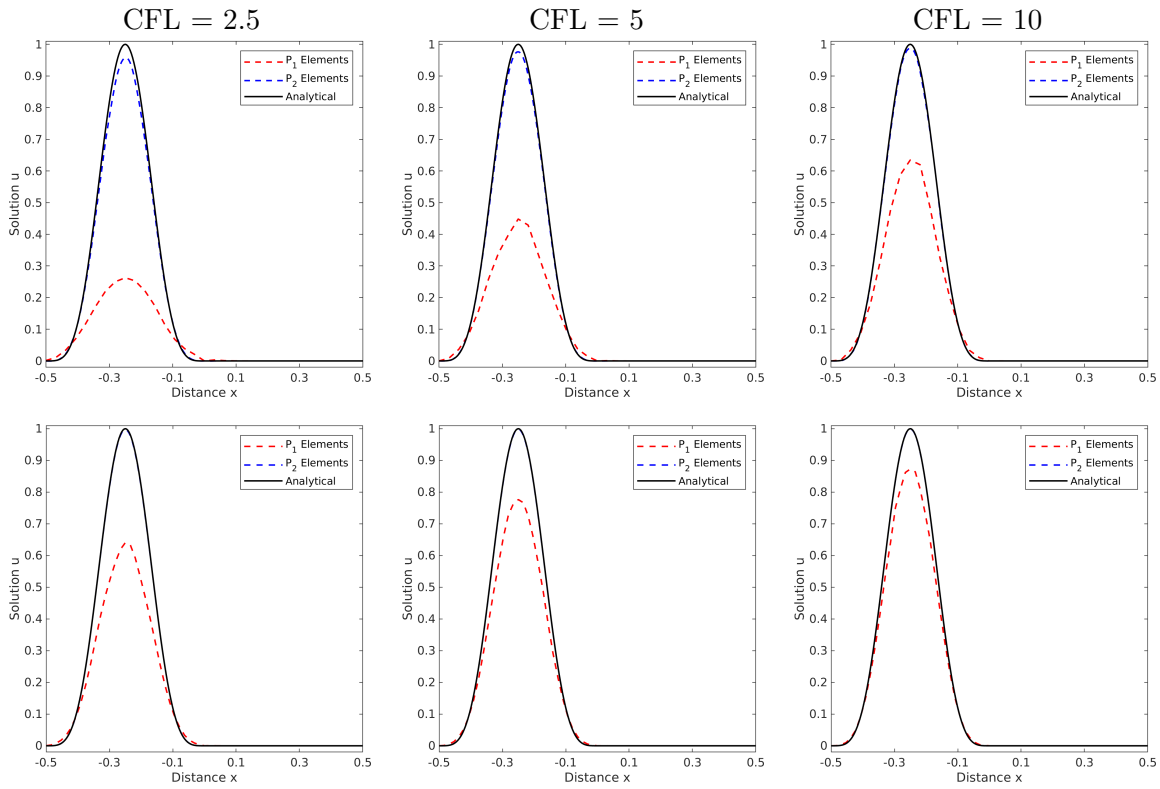

Figure 10: Cross-sections of the solution at $y = z = 0$ for a pulse in elliptical flow fields after 1 revolution using different values of CFL and meshes with $h = \frac{1}{64}$ (first row) and $h = \frac{1}{128}$ (second row).

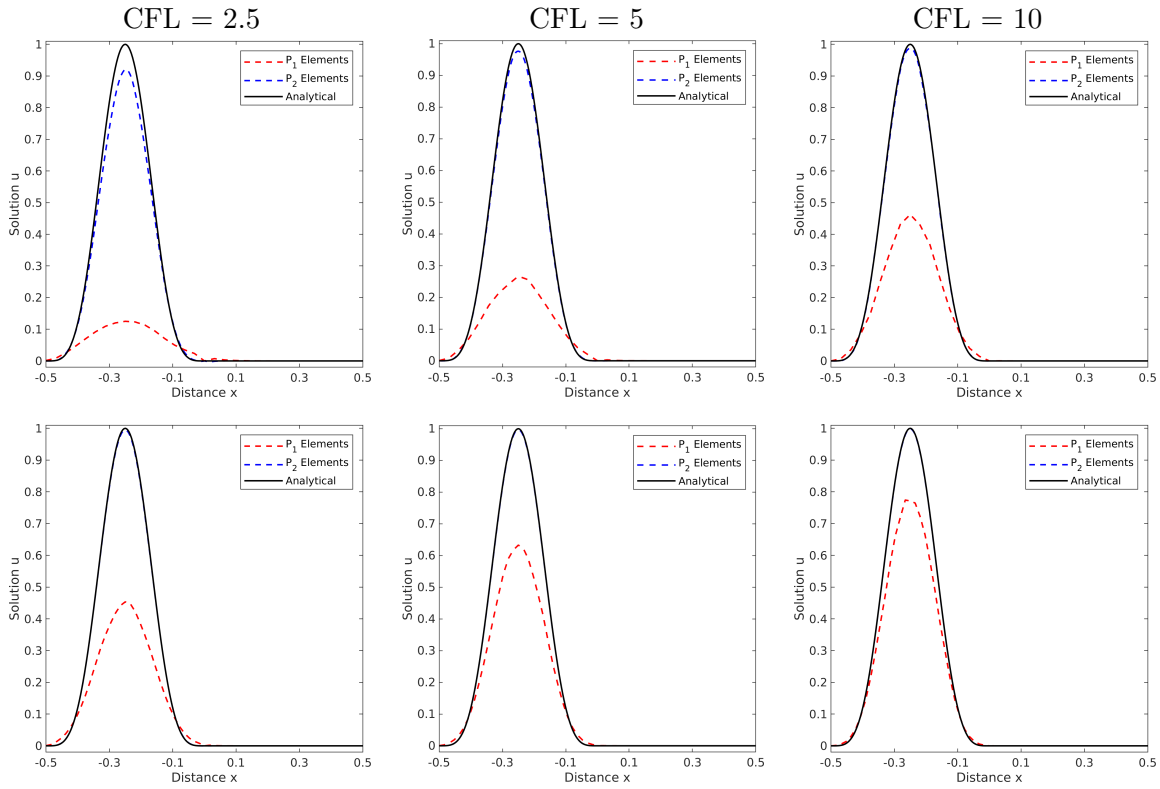

Figure 11: Same as Figure 10 but after 2 revolutions.

Table 3: Results for rotating a pulse in elliptical flow fields after 1 and 2 revolutions using different meshes and values of CFL. The analytical maximum is 1 and the CPU times are given in seconds.

After 1 revolution

		P_1 elements			P_2 elements		
CFL	h	Max	L^1-error	CPU	Max	L^1-error	CPU
2.5	$\frac{1}{32}$	0.044876	7.079468E-03	0.031	0.642729	2.394240E-03	0.282
	$\frac{1}{64}$	0.262814	4.997751E-03	0.262	0.958052	4.263776E-04	2.295
	$\frac{1}{128}$	0.640505	2.233033E-03	2.161	0.997189	7.976341E-05	20.046
5	$\frac{1}{32}$	0.126730	6.020042E-03	0.015	0.810252	1.437504E-03	0.140
	$\frac{1}{64}$	0.448218	3.476596E-03	0.133	0.956235	3.873386E-04	1.172
	$\frac{1}{128}$	0.776398	1.269638E-03	1.178	0.998302	6.639879E-05	10.946
10	$\frac{1}{32}$	0.286340	4.490564E-03	0.007	0.858095	9.906020E-04	0.073
	$\frac{1}{64}$	0.634328	2.139306E-03	0.072	0.986434	1.758627E-04	0.613
	$\frac{1}{128}$	0.872638	6.863190E-04	0.669	0.998905	5.062391E-05	6.409

After 2 revolutions

		P_1 elements			P_2 elements		
CFL	h	Max	L^1-error	CPU	Max	L^1-error	CPU
2.5	$\frac{1}{32}$	0.116924	6.694012E-03	0.061	0.494941	3.467405E-03	0.555
	$\frac{1}{64}$	0.126201	6.317412E-03	0.538	0.920680	7.284590E-04	4.471
	$\frac{1}{128}$	0.453411	3.457695E-03	4.336	0.994886	1.116419E-04	40.477
5	$\frac{1}{32}$	0.043784	6.860131E-03	0.030	0.703023	2.191195E-03	0.276
	$\frac{1}{64}$	0.266623	4.890499E-03	0.236	0.959980	4.103942E-04	2.327
	$\frac{1}{128}$	0.632906	2.167155E-03	2.379	0.997024	8.671431E-05	22.243
10	$\frac{1}{32}$	0.013168	7.093278E-03	0.016	0.809315	1.518063E-03	0.148
	$\frac{1}{64}$	0.462410	3.317591E-03	0.141	0.979549	2.702004E-04	1.243
	$\frac{1}{128}$	0.774063	1.241712E-03	1.330	0.998416	6.579213E-05	12.889

solutions for both P_1 and P_2 elements but the results obtained using P_2 elements are more accurate than those obtained using P_1 elements. Needless to say that for this convection-dominated situation, the Galerkin-characteristic finite element method does not diffuse the pulse or give spurious oscillations near the steep gradients. Our Galerkin-characteristic finite element method accurately approximates the solution to this three-dimensional advection problem.

3.3 Passive transport in a pipe

Our final concern is to ascertain the behavior of the Galerkin-characteristic finite element method to solve pure transport problems in pipelines. To this end we consider a passive transport of concentration in a deformed pipe subject to incompressible flow. The geometry of the pipe is illustrated in Figure 12 and a well developed velocity field shown in Figure 13 is assumed to be given by solving the incompressible Navier-Stokes equations. Initially, the concentration $c(x, y, z, 0) = 0$ and a release source f is included in

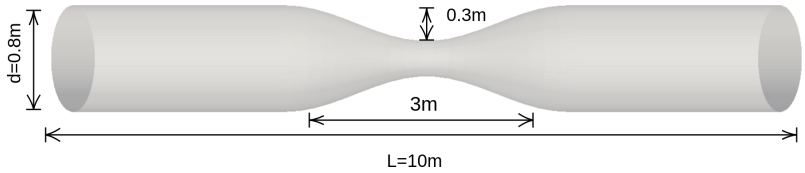

Figure 12: Geometry of the pipe used in our simulations.

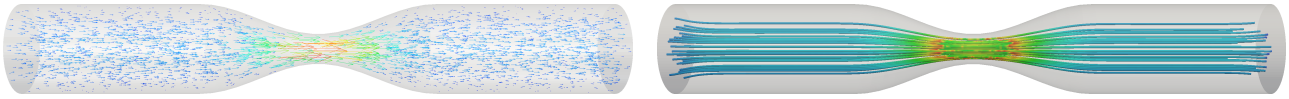

Figure 13: Velocity field (left) and streamlines (right) used for passive transport in a deformed pipe.

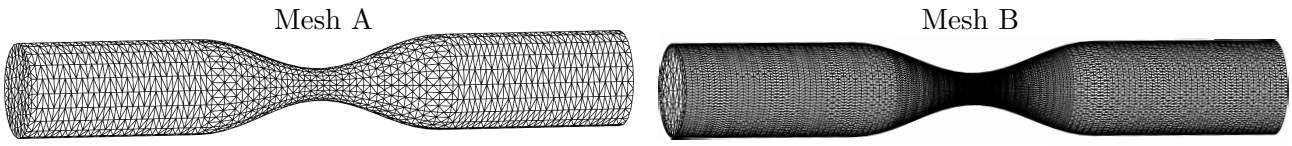

Figure 14: Computational meshes used in our simulations for passive transport in a deformed pipe.

Table 4: Mesh statistics and results for maximum concentration and CPU times (in seconds) for the problem of a passive transport in a deformed pipe.

Mesh	# of elements	# of nodes	Max	CPU
Mesh A	67989	106693	0.203681	20.223
Mesh B	907892	1270219	0.283702	345.764
Mesh C	3351827	4590175	0.287182	850.864
Reference	5301234	7205051	0.287438	1490.378

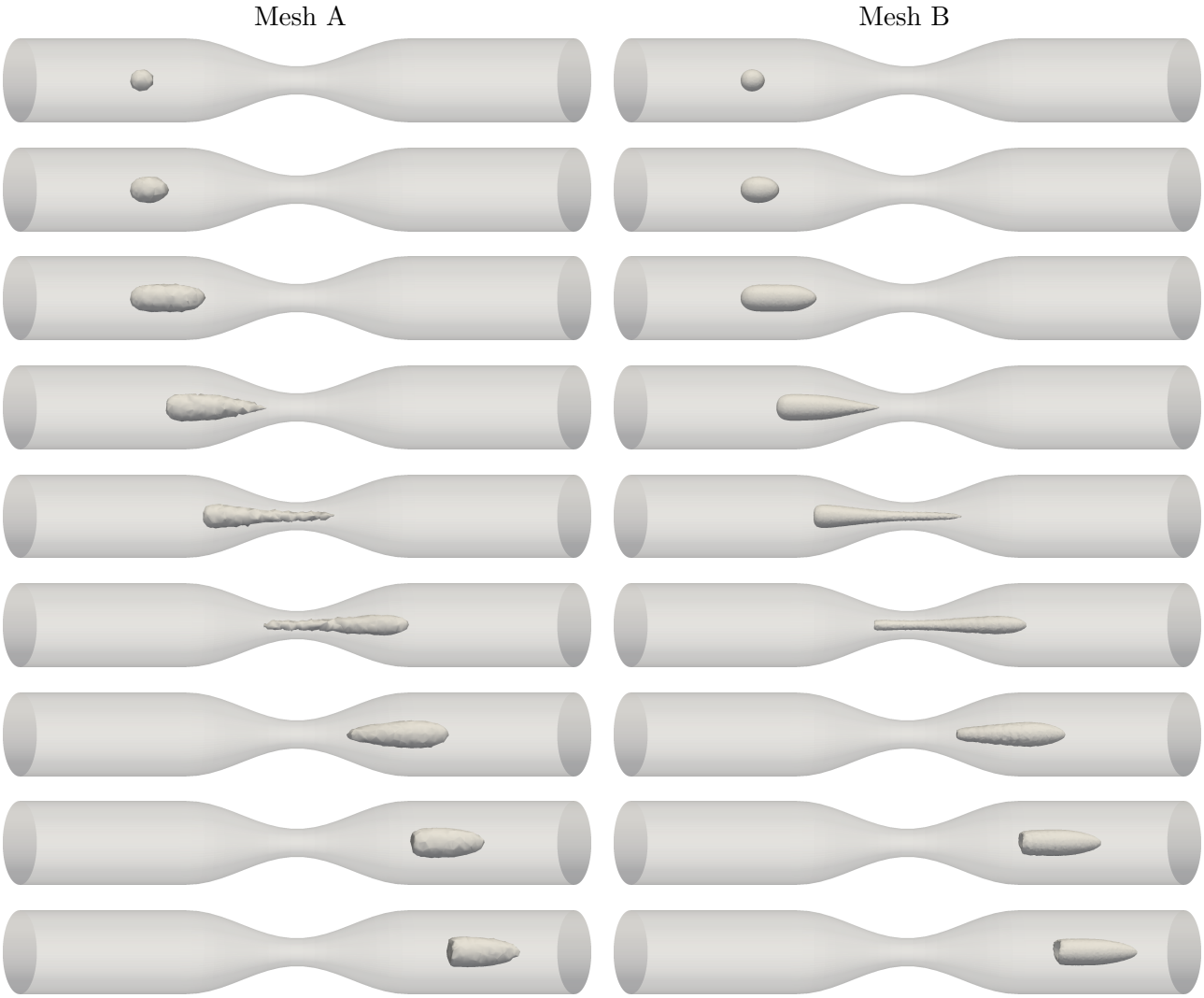

Figure 15: Numerical results obtained for passive transport in a deformed pipe using Mesh A (first column) and Mesh B (second column) at nine different instants. From top to bottom $t = 0.3\ s$, $0.5\ s$, $1\ s$, $1.5\ s$, $2\ s$, $2.5\ s$, $3\ s$, $3.5\ s$ and $4\ s$.

the system as

$$f(x,y,z,t) = \begin{cases} \exp\left(-\dfrac{(x-2)^2+y^2+z^2}{\sigma^2}\right), & \text{if} \quad t < 1s, \\ 0, & \text{if} \quad t \geq 1s, \end{cases}$$

where $\sigma^2 = 0.008$. In our computations, we use CFL $= 10$ and we consider a series of nonuniform meshes with tetrahedral finite elements as depicted in Figure 14. The corresponding statistics of elements and nodes are listed in Table 4. Note that Mesh C and the reference mesh are not included in Figure 14 because of their density which results in a heavily black plot. Figure 15 illustrates the concentration patterns at nine different times, namely $t = 0.3\ s$, $0.5\ s$, $1\ s$, $1.5\ s$, $2\ s$, $2.5\ s$, $3\ s$, $3.5\ s$ and $4\ s$ obtained using Mesh A and Mesh B. For better insight, we show in Figure 16 horizontal cross-sections of the concentration at $y = z = 0$. It is easy to see from both figures, that solutions obtained using the Mesh A are far from those obtained by the Reference mesh. Increasing the density of elements, the results for the Mesh B, Mesh C, and Reference Mesh are roughly similar. To further quantify the results for these meshes we summarize in Table 4 the computational times and maximum values of the concentration. Here, we present results obtained using the Galerkin-characteristic finite element method

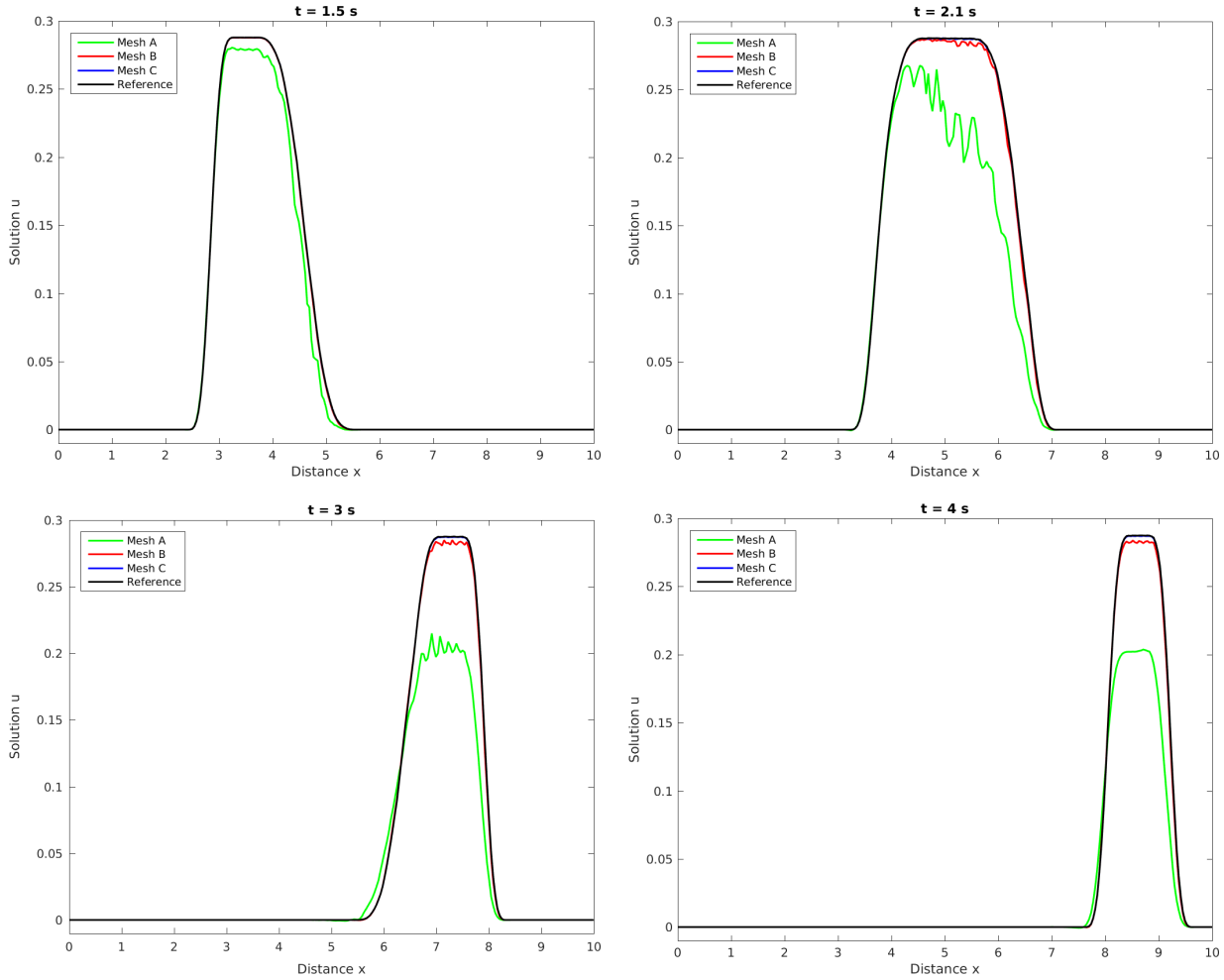

Figure 16: Cross-sections of the solution at $y = z = 0$ for the passive transport in a deformed pipe using different meshes and at four different times.

on the considered meshes including the reference mesh. As can be observed, there is little differences between the last two mesh levels. For instance, the discrepancies in the maximum values of concentration on Mesh B and Reference Mesh are less than 0.25%. This difference becomes less than 0.018% on meshes Mesh C and Reference Mesh. Therefore, bearing in mind the slight change in the results from Mesh B and Mesh C at the expanse of rather significant increase in CPU times, the Mesh B is believed to be adequate to obtain the results free of grid effects. From the computed results we can observe that the complicated transport structures in the pipe being captured by the Galerkin-characteristic finite element method. It is worth remarking that all these features have been achieved using time steps larger than those required for Eulerian-based methods in convection-dominated flows.

4 Conclusions

In this study we have presented a class of unconditionally stable Galerkin-characteristic finite element methods for solving convection-diffusion problems in three space dimensions. This method exploits the interesting features offered by both techniques to construct a highly accurate algorithm for numerical simulation of convection-diffusion problems. The important advantage of the proposed method is that, the convective term that has to be treated carefully in most of Eulerian-based finite element methods has been removed from the proposed method by using the modified method of characteristics to interpret

the transport nature of the equation. The favorable performance of the Galerkin-characteristic finite element has been demonstrated using a series of numerical examples including transport in pipelines. A comparison between linear P_1 and quadratic P_2 elements were also performed in the present study. The obtained results using the P_2 elements show good solution resolution and less numerical dissipation compared to the results obtained using the P_1 elements. This fact, as well as its favorable stability properties, make it an attractive alternative for three-dimensional convection-diffusion solvers based on Galerkin-characteristic finite element techniques. Finally, we should point out that due to the use of the Lagrangian coordinates, the Galerkin-characteristic finite element method requires more implementation work than the Eulerian methods which are relatively easy to formulate and to implement. The algorithms presented in this study can be highly optimized for vector computers, because they do not require nonlinear solvers and contain no recursive elements. Some difficulties arise from the fact that for efficient vectorization the data should be stored contiguously within long vectors rather than three-dimensional arrays. Future work will also concentrate on developing efficient Galerkin-characteristic finite element method for nonlinear convection-diffusion problems including incompressible Navier-Stokes equations in three space dimensions.

Acknowledgment. Financial support provided by the project CSIC under the contract M MTM2017-89423-P is gratefully acknowledged.

References

[1] A. Allievi and R. Bermejo. A generalized particle search-locate algorithm for arbitrary grids. *J. Comp. Physics*, 132:157–166, 1992.

[2] A. Murrone C. Le Touze and H. Guillard. Multislope MUSCL method for general unstructured meshes. *J. Comput. Phys.*, 284:389–418, 2015.

[3] C.N. Dawson. Godunov-mixed methods for advective flow problems in one space dimension. *SIAM J. Numer. Anal.*, 28:1282–1309, 1991.

[4] M. Dehghan. Numerical solution of the three-dimensional advection-diffusion equation. *Appl. Math. Comput*, 150:5–19, 2004.

[5] J. Douglas and T.F. Russell. Numerical methods for convection dominated diffusion problems based on combining the method of characteristics with finite elements or finite differences. *SIAM J. Numer. Anal.*, 19:871–885, 1982.

[6] M. El-Amrani and M. Seaid. Convergence and stability of finite element modified method of characteristics for the incompressible Navier-Stokes equations. *J. Numer. Math.*, 15:101–135, 2007.

[7] M. El-Amrani and M. Seaid. Numerical simulation of natural and mixed convection flows by Galerkin-characteristics method. *Int. J. Num. Meth. Fluids.*, 53:1819–1845, 2007.

[8] M. El-Amrani and M. Seaid. A finite element modified method of characteristics for convective heat transport. *Numer. Methods for Partial Differential Equations*, 24:776–798, 2008.

[9] M. El-Amrani and M. Seaid. A Galerkin-characteristics method for large-eddy simulation of turbulent flow and heat transfer. *SIAM J. Sci. Comp.*, 30:2734–2754, 2008.

[10] M.J. Peng H. Cheng and Y.M. Cheng. A hybrid improved complex variable element-free Galerkin method for three-dimensional advection-diffusion problems. *Engineering Analysis with Boundary Elements*, 97:39–54, 2018.

[11] L. Ali Khan and P.L.F. Liu. An operator splitting algorithm for the three-dimensional advection-diffusion equation. *Int. J. Numer. Meth. Fluids*, 28:461–476, 1998.

[12] K.W. Morton. *Numerical Solution of Convection-Diffusion Problems.* Chapman & Hall, 1996.

[13] N.-S. Park and J. A. Liggett. Application of taylor-least squares finite element to three-dimensional advection-diffusion equation. *Int. J. Numer. Meth. Fluids*, 13:759–773, 1991.

[14] O. Pironneau. On the transport-diffusion algorithm and its applications to the Navier-Stokes equations. *Numer. Math.*, 38:309–332, 1982.

[15] J.M. Qiu and C.W. Shu. Conservative high order semi-Lagrangian finite difference WENO methods for advection in incompressible flow. *J. Comput. Phys.*, 230:863–889, 2011.

[16] A. Robert. A stable numerical integration scheme for the primitive meteorological equations. *Atmos. Ocean*, 19:35–46, 1981.

[17] H. Rui and M. Tabata. A mass-conservative characteristic finite element scheme for convection-diffusion problems. *J. Sci. Comput.*, 43:416–432, 2010.

[18] M. Seaid. Semi-lagrangian integration schemes for viscous incompressible flows. *Comp. Methods in App. Math.*, 4:392–409, 2002.

[19] C. Shu and S. Osher. Efficient implementation of essentially non-oscillatory shock capturing schemes. *J. Comp. Physics*, 77:439–471, 1988.

[20] D. Sirajuddin and W.N.G. Hitchon. A truly forward semi-Lagrangian WENO scheme for the vlasov-poisson system. *J. Comput. Phys.*, 392:619–665, 2019.

[21] A. Staniforth and Côté J. Semi-lagrangian integration schemes for the atmospheric models: A review. *We. Rev.*, 119:2206–2223, 1991.

[22] E. Süli. Convergence and nonlinear stability of the lagrange-Galerkin method for the navier-stokes equations. *Numer. Math.*, 53:1025–1039, 1988.

[23] C. Temperton and A. Staniforth. An efficient two-time-level Galerkin-characteristics semi-implicit integration scheme. *Quart. J. Roy. Meteor. Soc.*, 113:1025–1039, 1987.

[24] D. Xiu and G.E. Karniadakis. A Galerkin-characteristics high-order method for Navier-Stokes equations. *J. Comp. Physics*, 172:658–684, 2001.

[25] X. Feng Y. Zhai and D. Lu. A novel method to deduce high-order compact difference scheme for the three dimensional semilinear convection-diffusion equation with variable coefficients. *Numer. Heat Transfer*, B 63 (5):425–455, 2013.